Design of ultra-high speed optical beam chopper rotors

Timon Achtnich[1], Philipp Bühler[1]

Abstract

High-speed beam choppers usually require a fast circumferential and rotational speed and vacuum operation, for which the Celeroton magnetic bearing systems are well suited. The chopper rotor requires a stepwise design process, which is presented in this white paper, including requirements definition, mechanical and rotor dynamic design. It is shown that circumferential speeds up to approximately 1 km/s are feasible for discs made from Titanium and jitters of smaller than 4 ns can be achieved with such a design and Celeroton magnetic bearing systems.

1   Introduction

High-speed beam choppers are required to stimulate a sample with a frequency modulated beam [1] or when single pulses have to be isolated out of pulse stream [2]. Usually fast opening and closing times are preferred or required, requiring a fast circumferential speed for the commonly used rotating chopper disks. High circumferential speeds are reached by increasing the rotational speed or the diameter of the chopper disc (or both) but there is limit caused by the rotor material's tensile strength, the generated losses, and the achievable rotational speed of the controller. This white paper describes the main aspects to be considered when designing an ultra-high speed chopper rotor.

1.1   Celeroton's magnetic bearing technology

Chopper rotors, specifically those running at elevated speeds, are usually operated in vacuum to avoid excessive air friction losses, also called windage losses. Therefore, often magnetic bearings are employed as they are vacuum compatible. Celeroton's magnetic bearing systems are well suited for ultra-high speed optical beam chopper applications and feature a modular design. The magnetic bearing controller family CC-AMB covers a high range of magnetic bearing and motor power demands. The magnetic bearing motor CM-AMB is also designed with building blocks that allow fast and easy adaption to different rotor and chopper disk geometries and sizes. The magnetic bearing controllers and motors can provide ultra-high rotational speeds up to 400 krpm, low vibration position control of the rotor and a stable rotational speed control for minimal jitter.

Application specific rotor designs enable to fulfil custom specific needs and with that, create a unique magnetic bearing system.

The design aspects presented in this white paper are mainly independent of the specific magnetic bearing technology applied.

1.2   Terms

For a better understanding, some important terms are defined:

Disc   Part of the rotor with slots (or polygon surface)

Rotor   Entire rotor consisting of the disc, rotor hubs, magnets, etc.

Beam   Optical beam chopped by the disc

1.3   Time-behaviour of chopped beam

The first step of designing a chopper rotor is defining the required time-behaviour of the chopped beam.

The time-behaviour of a chopped beam can be characterized by the following parameters, also depicted in Figure 1.

- T: Period of the chopper frequency
- f_c: Chopper frequency $f = \frac{1}{T}$
- t_o: Opening time
- t_c: Closing time
- t_d: Dwell time or 100% exposure time
- D: Duty cycle, given by $D = \frac{t_d + t_c}{T}$

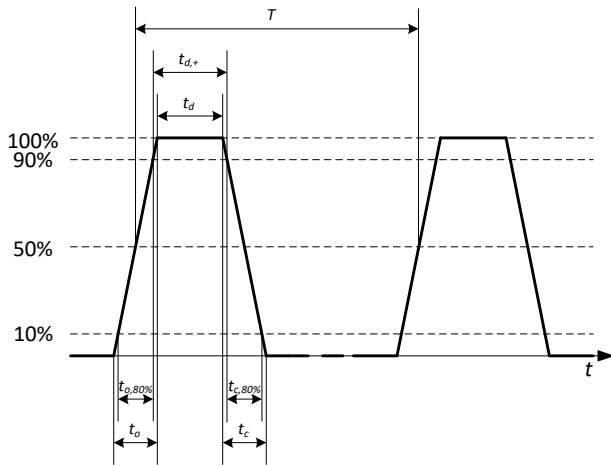[1] Celeroton AG, Industriestrasse 22, 8604 Volketswil, Switzerland

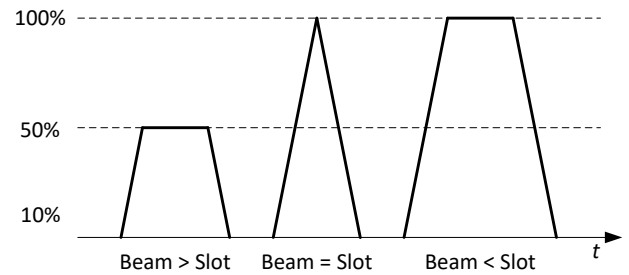Figure 1: Graphical representation of time-behaviour of chopped beam.

Figure 2: Transmission function of a parallel beam versus time for three different cases: Left: Beam size larger than slot opening; Middle: Beam size equal to slot opening; Right: Beam size smaller than slot opening [3].

Assuming constant rotational speed, the opening and closing time are identical, thus in the following only the closing time is used.

In literature, different definitions for the opening, closing and dwell time are used. For the calculation the opening time t_o, the closing time t_c and the dwell time t_d according to Figure 1 are used. When these times are measured, it is better to measure the time span between 10% and 90% of the amplitude of the measured beam denoted as $t_{o,80\%}$ for the opening time, $t_{c,80\%}$ for the closing time and between 90% amplitude of the rising edge and 90% of the falling edge for the dwell time denoted as $t_{d,+}$ as the detection of 0% and 100% amplitude is inaccurate due to noise on the measured signals.

The slots of a chopper can be designed to have a lower, equal or larger size than the beam. A smaller slot than the beam results in a trapezoidal transmission function with limited intensity in the plateau (Figure 2 left). With an equal size of the slot, the beam should be avoided as the amplitude of the chopped beam becomes sensitive to small jitters in the chopper disc (Figure 2 middle). When the slot is larger than the beam, the transmission function is again trapezoidal but will not limit the intensity of the beam (Figure 2 right).

1.4 Chopper topology

Chopping a beam is possible with two main topologies as shown in Figure 3. A disc shaped chopper with the slots and the beam parallel to the rotation axis is defined as a parallel topology. A disc shaped chopper with the slots and the beam perpendicular to the rotation axis is defined as a perpendicular topology.

A first subclass of the perpendicular topology is achieved when the rotor material outside of the slots of perpendicular design is removed resulting in a polygon shaped rotor.

A second sub class of the perpendicular topology is achieved when the slot is moved into the centre, hereafter named as perpendicular centre topology.
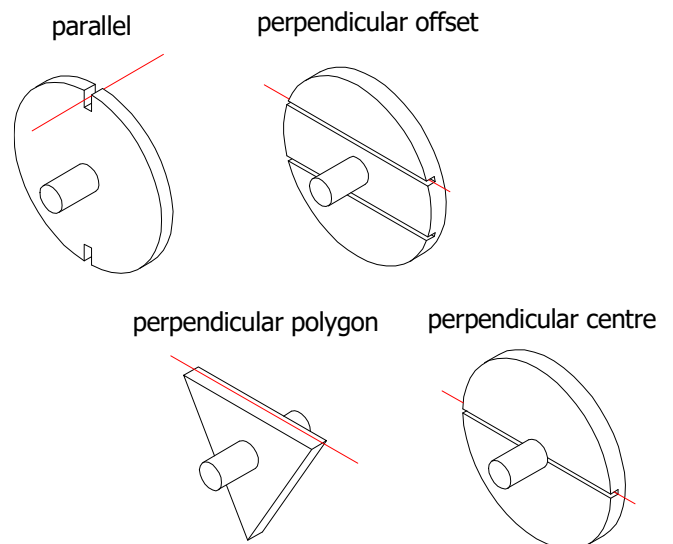

Figure 3: Schematic view of parallel and perpendicular chopper topologies mentioned in [4]. The perpendicular polygon and the perpendicular centre topology are sub-types of the perpendicular offset topology.

In a parallel design, the beam starts passing a slot, when the leading edge of a slot is at the outer position of the beam diameter. In a perpendicular channel-type design, the beam starts passing a slot not before the edge (both sides) of a slot are in the centre of the beam. Hence, the opening and closing time are shorter by a factor of two compared to a parallel design with the same diameter and rotational speed. This is a big advantage, when the opening and closing time have to be minimized. It is defined with the closing time factor k_{t_c} given in Table 1. Higher values of k_{t_c} are possible in perpendicular channel topologies by using a bundle of narrow channels in parallel separated by thin walls. A polygon chopper does not feature this reduced opening and closing time, even though being a sub class of the perpendicular chopper, as a polygon chopper does not have this channel-type behaviour.

A perpendicular centre topology has the advantage, that the beam is travelling twice through the same slot during one rotation and with that, the chopper frequency is doubled at the same rotational speed compared to a parallel design or a perpendicular design with slots offset from the rotation axis. This property is defined with the chopper frequency factor k_{f_c} given in Table 1.

Topology	k_{f_c}	k_{t_c}
parallel	1	1
perpendicular offset	1	2
perpendicular polygon	1	1
perpendicular centre	2	2

Table 1: Chopper frequency factor k_{f_c} closing time factor k_{t_c}, and minimum slot radius $r_{s,min}$ for different chopper topologies.

Having the goal of minimizing the opening and closing times and maximizing the chopper frequency, the perpendicular centre topology might be the best solution. However, the slots weaken the rotor at the most stressed area of the rotor in the centre. Chopper rotors with perpendicular centre topology operated at the material's strength limit will achieve a lower maximum rotational speed compared to chopper rotors with parallel topology. With that, the benefit of the doubled chopper frequency and halved opening and closing time of a perpendicular centre topology is diminished. Which topology is best suited depends on the specific design, on the number of slots and the slot size.

The parallel and perpendicular centre topology shown in Figure 3 are designed with two slots. Having more than two slots is possible and is mainly defined by the application. Choppers with only one slot are also possible but will add unbalance to the rotor by design. Balancing of the rotor at dedicated balancing planes can compensate the unbalance of a one slot chopper design.

1.5 Synchronization of choppers

In most experiments it is necessary to synchronize the chopper speed as well as the position to an external reference signal. Celeroton's magnetic bearing controllers CC-AMB have a built-in phase lock loop (PLL) for this purpose. This facilitates the integration of the chopper into the application, as no external PLL control is needed.

This PLL capability can also be used to synchronize two choppers with each other, which enables higher freedom on the time behaviour of the chopped beam. Sometimes the optimal duty cycle for an experiment is not known at the requirements phase of the chopper design or an adjustable duty cycle is desired. With a single chopper, the duty cycle is given by the chopper disc design. It can only be altered, when the rotor is changed or a rotor with numerous but different slot patterns is used. A much more flexible approach for this case is to use two synchronized choppers in series. Then the duty cycle can be adjusted with a stepless behaviour, by changing the phase of the two choppers running at the same rotational speed.

Applications requiring a low duty cycle and a large slot opening will end up with a comparably large disc diameter. Instead, two synchronized choppers with a smaller disc compared to the single chopper topology can be used. Where the first chopper is running with the same circumferential speed as the single chopper (and maintaining the opening and closing time) and the second chopper is operated at lower speed to reduce the frequency of the first chopper.

2 Design of a chopper disc

Besides the parameters describing the time behaviour of a chopped beam given at the beginning of section 1.3, the following parameters are important for the chopper design.

- Thickness of the chopper disc to stop the beam
- Thermal heating of the chopper disc by the energy of the beam

- Beam diameter, slot geometry and size

The slots and the thickness of a disc are dimensioned according to Figure 4.
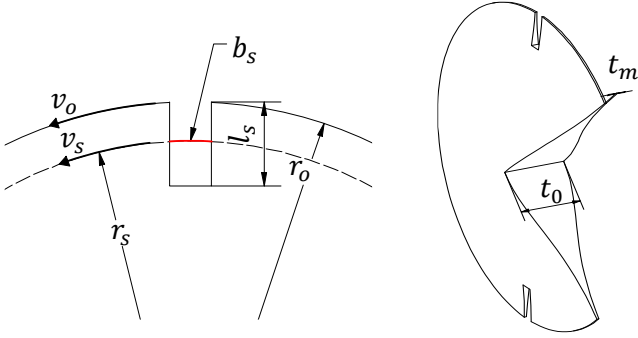

Figure 4: Left: Dimensioning of slot of a parallel chopper disc; Right: thickness of a chopper disc shown for a Stodola shaped chopper disc.

The following five mechanical parameters of a chopper define the time-behaviour of a chopped beam:

- r_s radius of the slot circle
- N the number of slots
- b_S the arc length of the slot
- f the rotational frequency of the chopper
- d_B diameter of the beam

The relation between the time-behaviour of the chopped beam and the mechanical parameters of a chopper disc are established with the subsequent formulas.

The chopper frequency f_c is given by

$$f_c = f \cdot N \cdot k_{f_c}. \tag{1}$$

where f is the rotational frequency, N the number of slots on the chopper rotor and k_{f_c} the chopper frequency factor according to Table 1. The rotational frequency f is be defined by the angular velocity $\omega = 2 \cdot \pi \cdot f$ or by the rotational speed $n = 60 \cdot f$.

The duty cycle D is given by

$$D = f_c \cdot (t_d + t_c), \tag{2}$$

where t_d ist the dwell time and t_c the closing time defined as

$$t_c \approx \frac{d_b}{v_s \cdot k_{t_c}}, \tag{3}$$

where v_s is the circumferential speed at the slot's radius, d_b the beam diameter and k_{t_c} the closing time factor given in Table 1. Equation (3) is an approximation for the exact calculation of the beam's arc length, that is given when the beam completely passes one slot edge. If $d_b \ll r_s$ then (3) is a good approximation.

The circumferential speed v for the radius r is given by

$$\begin{aligned} v_s &= \omega \cdot r_s, \\ v_o &= \omega \cdot r_o, \end{aligned} \tag{4}$$

Where r_s denotes the slot radius and r_O the outer radius of the disc, which is typically defined as

$$r_o = r_s + \frac{l_s}{2}, \tag{5}$$

with l_s being the slot length in radial direction.

The arc length of the slot b_S is given by

$$b_s = v_s \cdot (t_d + t_c). \tag{6}$$

Instead of defining the mechanical parameters of a chopper disc directly during the design, it is often preferred to define the time-behaviour of a chopped beam by the parameters given at the beginning of section 1.3.

Furthermore, the slot radius r_s has to fulfil the following equation

$$r_s \geq r_{s,min}, \tag{7}$$

where for all perpendicular chopper topologies the minimum slot radius is $r_{s,min} = 0$ mm and for the parallel chopper topology the minimum slot radius is $r_{s,min} = r_{st} + r_b$, where r_{st} is the stator outer radius.

2.1   Material's strength

The rotational speed of a rotor is, among others, limited by the material's strength. For the disc designs in the following sub-sections, high-grade Titanium is used with the material parameters according to Table 2.

Material parameter	Symbol	Value	Comment
Yield strength	σ_{max}	700 MPa	at $T = 200°$ and including some margin
Density	ρ	4400 kg/m³	
Poisson's ratio	ν	0.35	

Table 2: Material parameter of high-grade Titanium.

The calculations in the following two sub-sections are stated for discs without any slots. In most cases, slots weaken a disc. Hence, for a detailed design the maximum stress for a slotted disc must be identified by a finite element method (FEM) simulation.

2.1.1 Uniform flat disc

The maximum stress σ for a uniform flat disc occurs in the centre of a rotor and is given by

$$\sigma = \frac{1}{8} \cdot (3 + v) \cdot \rho \cdot \omega^2 \cdot r_o^2, \tag{8}$$

where v is the Poisson's ratio, ρ the material density, ω the angular velocity and r_o the outer radius of the rotor. The stress in the material is quadratically increasing with the angular velocity and the outer radius of the disc and thus with the circumferential speed. Substituting the peripheral speed $v_o = \omega \cdot r_o$ we obtain

$$\sigma = \frac{1}{8} \cdot (3 + v) \cdot \rho \cdot v_o^2. \tag{9}$$

Solving (9) for the circumferential speed we get

$$v_o = \sqrt{\frac{8 \cdot \sigma}{(3 + v) \cdot \rho}}. \tag{10}$$

A good choice for rotor's material is high-grade Titanium, which has high strength and is lightweight. The maximum circumferential speed for a uniform flat disc according to (10) is $v_{max} = 616$ m/s.

2.1.2 Evenly stressed disc

A uniform flat disc is not the optimal shape to achieve maximum circumferential speed. The thickness of the disc t over the radius r can be changed such that the radial and circumferential stress are equal and constant overall the whole disc, as defined by Stodola [5]. The shape of the evenly stressed disc is defined by

$$t = t_0 \cdot e^{-\frac{\rho \cdot \omega^2 \cdot r^2}{2 \cdot \sigma}}, \tag{11}$$

where t_0 is the thickness of the disc at the centre ($r = 0$). The evenly stressed disc has the profile of a Gauss error curve. The radius of the rotor is extending to infinity and with that infinite circumferential speed and reaching zero thickness. The shape of the disc according to (11) with $\omega = 2 \cdot \pi \cdot 6$ kHz and $t_0 = \{10,20,30,40,50\}$ mm, is shown in Figure 5.
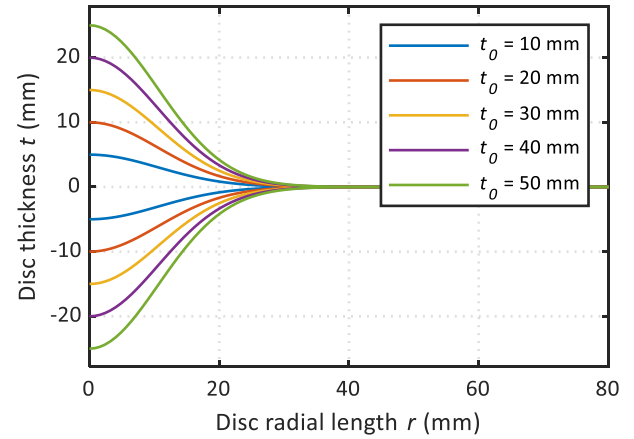

Figure 5: Shape of Stodola disc for different disc thickness t_0 at the centre. The ordinate of the plot coincides with the axis of rotation.

For a real application, the rotor has to be truncated at a given thickness $t = t_m$ or a given radius $r = r_m$ for practical purposes and the application may require a minimal disc thickness to properly stop the beam (e.g. X-ray applications). With that, the stress at the disc edge is reduced to zero but if $t_m \ll t_0$ then the stress at the centre is only changed marginally.
Solving (11) for the circumferential speed, we get

$$v = \sqrt{\ln \frac{t_0}{t} \cdot \frac{2 \cdot \sigma}{\rho}}. \tag{12}$$

The circumferential speed is plotted in Figure 6 (solid lines) for $t_0 = \{10,20,30,40,50\}$ mm as a function of the disc thickness at the tip t_m. It can be seen that circumferential speeds above 1 km/s can be achieved with the chosen material parameters from high-grade Titanium. However, if t_m is relatively close to t_0 the maximum circumferential speed can even be lower than for a uniform flat disc as the material is not used optimally (blue curve in Figure 6).
To optimize this, the disc can be extended with constant thickness t_m from radius r_m until the force $F = \sigma_{max} \cdot dA$ is reached at the surface $dA = t \cdot r_m \cdot d\theta$ at radius r_m. The force acting on the surface A is given by

$$F = \int_{r_m}^{r_e} \omega^2 \cdot r^2 \cdot \rho \cdot t \cdot d\theta \cdot dr, \tag{13}$$

where $d\theta$ is an infinitesimal step in angular direction, dr an infinitesimal step in radial direction and r_e the end radius of the disc. Solving (13) for r_e yields

$$r_e = \sqrt[3]{\frac{3 \cdot r_m \cdot \sigma}{\omega^2 \cdot \rho} + r_m^2}. \qquad (14)$$

Rotors of this type are hereafter named as 'Stodola shape extended'. The increased circumferential speed is seen, when comparing the dashed lines ('Stodola shape extended') with the solid lines ('Stodola shape truncated') in Figure 6.

Examples of the three different rotor shapes discussed are shown in Figure 7. The disc's radius and the circumferential speed of the 'Stodola shape extended' is increased by 18% compared to 'Stodola shape truncated' and in this example reaching a circumferential speed above 1 krpm/s.
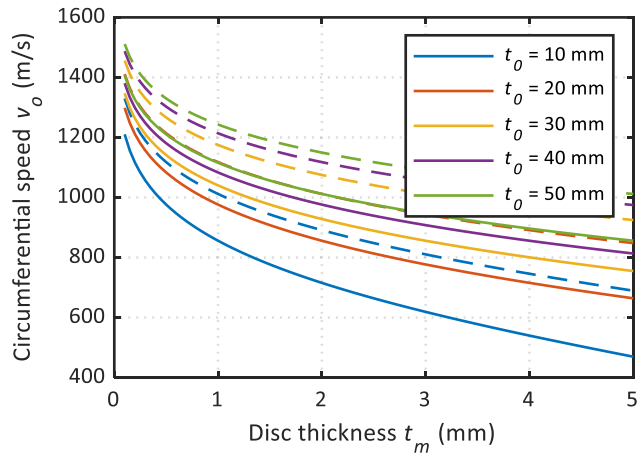

Figure 6: Circumferential speed v_o at the disc end. Solid lines are for type 'Stodola shape truncated' and dotted lines for type 'Stodola shape extended'.
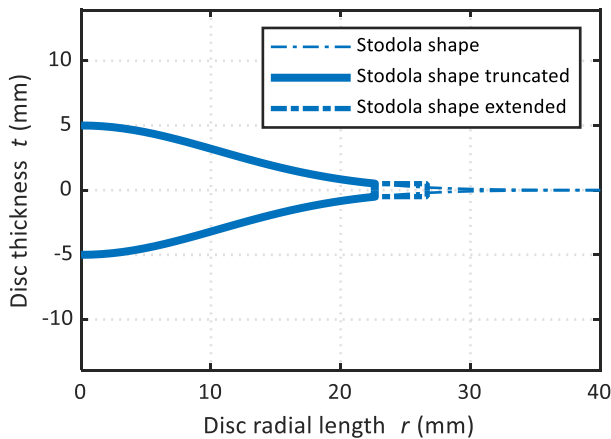

Figure 7: Shape of Stodola disc for three different shapes at the disc tip all starting with thickness $t_0 = 10$ mm and ending with $t_m = 1$ mm.

2.2 Rotordynamics

Besides the mechanical strength of the rotor, also the rotordynamics is important for the operation of the rotor, especially at ultra-high speeds.

2.2.1 Eigenfrequencies

The eigenfrequencies of a rotor are best analysed with a FEM model. The rotational frequency of the rotor f has to be smaller than the frequencies of the bending modes f_e

$$f < f_e. \qquad (15)$$

For a first estimation, the eigenfrequencies of the free rotor can be calculated.

There exist applications where the operation of the rotor is at higher speed than the eigenfrequencies of the bending modes. During acceleration of the rotor the rotational frequency will pass through these eigenfrequencies. This requires a high dynamic force capacity of the magnetic bearing and advanced control techniques. Eigenfrequencies above rotational frequency should be prevented if they are not necessary.

2.2.2 Moments of inertia

The nutation frequency ω_{nut} of the rotor should be different from the frequency of rotation Ω. Otherwise, the nutation frequency is excited by unbalance, which is always present. The nutation frequency for a rotor is

$$\omega_{nut} = \frac{I_z}{I_{x,y}} \cdot \Omega, \qquad (16)$$

where zero magnetic stiffness is assumed. $I_{x,y,z}$ denotes the principal moments of inertia around the x,y,z-axis, where z is the axis of rotation. Hence, the following equation must be fulfilled

$$\frac{I_z}{I_{x,y}} = \gamma \neq 1. \qquad (17)$$

In order to get some safety margin, the safe range is usually set to:

$$\gamma < 0.8 \; or \; \gamma > 1.2 \qquad (18)$$

For the analysis of the ratio of the moments of inertia γ the whole rotor and not only the disc has to be considered. The rotor's hubs might have only a minimal impact on I_z but often have a bigger impact

on $I_{x,y}$. The calculation of the rotor's hub inertias is trivial but as it depends on the geometry it would require a lot of parameters when given in a general formula. The calculation of the moments of inertias for the entire rotor is best done with a computer aided design (CAD) tool. In this report, the analytical calculation of the moment of inertias is only given for the disc itself, in order to discuss the different extrema.

The moment of inertia I_z for a 'Stodola shape truncated' disc is calculated according to (19).

$$I_z = \frac{k_1}{2 \cdot k_2^2} \cdot \left(1 - (k_2 \cdot r^2 + 1) \cdot e^{-k_2 \cdot r^2}\right),$$
$$k_1 = t_0 \cdot \rho \cdot 2 \cdot \pi, k_2 = \frac{\rho \cdot \omega^2}{2 \cdot \sigma} \tag{19}$$

When the radius of the disc is extended to infinity as for a 'Stodola shape' disc, then (19) simplifies to

$$I_z(r \to \infty) = \frac{k_1}{2 \cdot k_2^2} = \frac{4 \cdot \pi \cdot t_0 \cdot \sigma^2}{\rho \cdot \omega^4}. \tag{20}$$

The moment of inertia $I_{x,y}$ for a 'Stodola shape' disc is calculated by

$$I_{x,y} = \frac{1}{2} \cdot I_z + \frac{\pi \cdot \rho \cdot t_0^3}{9 \cdot k_2}. \tag{21}$$

In Figure 8 the ratio of moments of inertia γ is plotted in function of the rotor thickness at the centre t_0. A ratio of the moments of inertia tending to two corresponds to a disc-like rotor, whereas a rotor with a ratio of moments of inertia tending to zero corresponds to a rod-like rotor. A rotor with a ratio of moments of inertia close to one behaves like a ball shaped rotor, which must be prevented (shaded area in Figure 8).

No direct conclusion of non-permitted disc thickness t_0 can be drawn from Figure 8 as the ratio of moments of inertia γ has to be analysed for the entire rotor and not only for the disc, as mentioned earlier. Nevertheless, with Figure 8 the workflow of identifying the allowed disc thickness t_0 is illustrated and a considerable range of disc thickness t_0 might not be feasible.
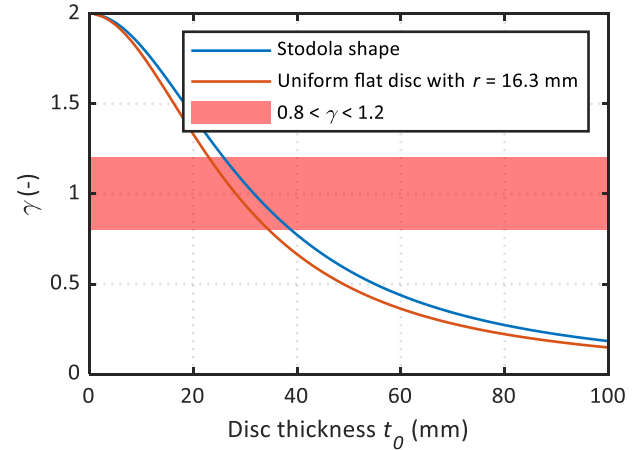

Figure 8: Ratio of moments of inertia γ in function of the disc thickness at the centre t_0.

2.3 Kinetic energy

The kinetic energy of a disc is given by the following equation

$$E = \frac{1}{2} \cdot I_z \cdot \omega^2. \tag{22}$$

For the uniform flat disc this yields to

$$E_{flat} = \frac{1}{4} \cdot \pi \cdot t_0 \cdot \rho \cdot \frac{v_0^4}{\omega^2}. \tag{23}$$

and for the Stodola shaped disc

$$E_{Stod} = \frac{2 \cdot \pi \cdot t_0 \cdot \sigma^2}{\rho \cdot \omega^2}. \tag{24}$$

For flywheel applications, the kinetic energy should be maximized. However, for chopper applications, the kinetic energy should be minimized due to safety reasons.

For both, a 'Stodola shaped disc' and a uniform flat disc, at constant circumferential speed, the angular velocity must be maximized to limit the energy build-up in the disc as given in (24).

This relation is explained with two choppers A and B, both having a uniform flat disc and the same chopper frequency f_c but chopper A is rotating at $n = 400$ krpm and chopper B rotating at $n = 200$ krpm. To maintain the same chopper frequency f_c the disc of chopper A has $N = 2$ slots, whereas the disc of chopper B has $N = 4$ slots. To maintain the same closing time t_c, hence having the same circumferential speed, the radius of the slot circle r_s in chopper B has to be twice the slot circle radius of chopper A. For simplicity the disc outer radius

is set to $r_o = r_s$. The ratio of the rotor's kinetic energy is given by

$$\frac{E_B}{E_A} = \frac{r_B^4 \cdot \omega_B^2}{r_A^4 \cdot \omega_A^2} = \frac{(2 \cdot r_o)^4 \cdot \left(\frac{\omega}{2}\right)^2}{r_o^4 \cdot \omega^2} = 4,$$

hence, for doubling the rotors outer radius r_o the kinetic energy has increased by factor of four.

However, the angular velocity cannot be increased infinitely. The achievable angular velocity is limited by the rotational speed dependent losses and the design of the magnetic bearing controller – given that the rotor is designed for the required rotational speed. Celeroton's magnetic bearing systems are optimized for ultra-high rotational speeds up to $n = 400$ krpm ($f = 6.6$ kHz) and with that bring a major advantage for chopper designs.

2.4 Optimum design

The workflow for designing a chopper disc strongly depends on the given boundary conditions. Figure 9 shows the flow chart for one typical set of parameters, namely: f_c, t_c, D, d_B, and the material's parameters σ, ρ.

In the following example the customer's requirements are:
$f_c = 200$ kHz, $t_c = 1$ μs, $D = 0.5$, $d_B = 1$ mm, $t_0 = 10$ mm, $t_m = 3$ mm, $l_s = 3$ mm, $\sigma = 700$ MPa, $\rho = 4400$ kg/m³.

The circumferential speed at the slot is calculated to $v_s = 1$ km/s, the maximum circumferential speed for a Stodola shaped disc is $v_{max} = 619$ m/s, which is lower than the desired speed. Therefore, the closing time is increased to $t_c = 2$ μs, yielding a circumferential speed of $v_s = 500$ m/s, which is feasible. The rotational frequency for $N = 1$ is calculated to $f = 200$ kHz, which is not feasible and hence the number of slots is set to $N = 50$. With that, we get $f = 4$ kHz. The dwell time is $t_d = 1.5$ μs and the arc length of the slot $b_s = 1.3$ mm. Finally, the radius of the slot is $r_s = 20$ mm, the outer radius of the disc $r_o = 21$ mm, the outer circumferential speed $v_o = 538$ m/s, which is still below the maximum circumferential speed. The ratio of moments of inertia γ for the entire rotor need investigation, which is not part of this basic example.

If not all requirements can be met, as in the example above, it has to be thoroughly checked to find which requirement can be relaxed.
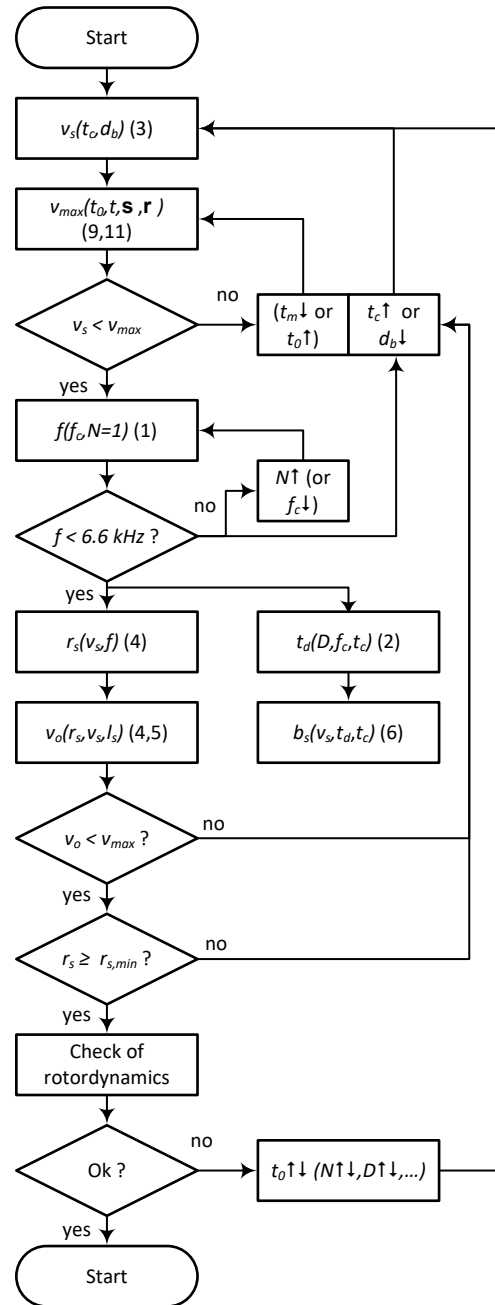

Figure 9: Flow chart for calculating geometric parameters for a chopper disc, when the following main parameters are given: $f_c, t_c, D, d_B, \sigma, \rho$. The up and down arrows indicate, if a parameter has to be increased or decreased and the number in round brackets indicate the equation used for the calculation.

3 Jitter

Having a low jitter on the time-behaviour of a chopped beam is often very important for the chopper application and a quality feature of a chopper. The jitter originates on the one hand from the manufacturing inaccuracy of the disc and on the other hand from the operation.

3.1 Manufacturing inaccuracy

For the manufacturing inaccuracy, it mainly comes from the following influences:

- Inaccuracy of the slot size
- Inaccuracy of the slot position
- Non congruency between the centre of the slot circle and the centre of rotation

The inaccuracy of the slot size and the slot position cannot be corrected once the disc is manufactured. Therefore, it is very important to have a precise manufacturing of the slots into the disc. With wire electrical discharge machining (EDM) position accuracies of below 5 µm can be achieved based on our experience. The inaccuracy of the slot size and slot position generates a jitter in time, which is inversely proportional with the circumferential speed. In Figure 10 the jitter for a slot displacement by ± 2.5 µm (or slot size inaccuracy) is shown. For circumferential speeds above 650 m/s the jitter is below 2 ns.
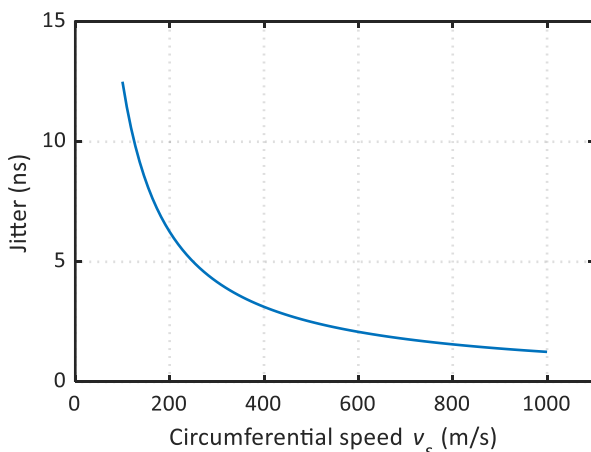

Figure 10: Jitter due to manufacturing inaccuracy of the slot size and slot position in function of the circumferential speed.

Due to manufacturing inaccuracies and inhomogeneity of the material's density, every rotor has some unbalance. A free rotor always rotates around the centre of inertia and not around the centre of geometry. In a magnetic bearing system most often a notch filter with the notch at the frequency of rotation allows the rotor to rotate around the centre of inertia. Rotation around the centre of geometry would require counteracting the centrifugal forces caused by unbalance, which increase with the square of the rotational speed.

The slots are manufactured with the alignment to the geometric centre. Therefore, standard balancing of the disc most often lowers the jitter. However, there is also a mismatch between the centre of the slot circle and the centre of geometry. Therefore, a more promising approach is to balance the rotor such that the centre of the slot circle aligns as good as possible with the centre of inertia. This process requires advanced post processing of the measured time-behaviour of the chopped beam to determine the required balancing.

The jitter due to the residual unbalance cannot be specified in general and is given by the balancing process.

3.2 Operation of the chopper

The operation of the chopper can add additional jitter to the time-behaviour of the beam and is mainly caused by:

- Instability of the rotational speed
- Position control of the rotor

The rotational speed in Celeroton's magnetic bearing motors is closed loop controlled by measuring the rotational position of the rotor and deducing the actual speed out of this measurement. This allows an accurate speed control. Remaining instabilities of the rotational speed are mainly caused by noise on the rotational position and current measurements. Filtering of these measurements and the low pass behaviour of every rotor results in a precise and robust speed control.

The radial and axial position of a magnetic bearing rotor are controlled to the geometric origin of the rotor. Any displacement of the rotor will cause additional jitter on the time-behaviour of the beam. In Celeroton's magnetic bearing motors these displacements are minimized by high sampling rates (400 kHz) of the position measurements combined with low pass filtering of these signals. As explained above, the digital notch filter on the position signals allows the rotation of the rotor around its centre of inertia. When the rotor is balanced such that the centre of the slot circle coincides with the centre of inertia, then a displacement between the centre of geometry and the centre of inertia will not add any jitter to the time-behaviour of the chopped beam.

The jitter of a laser beam (FP-Mini-520 from Laser Components) chopped by the magnetic bearing motor CM-AMB with a chopper disc and recorded with a photodiode (ODD-1WB by Opto Diode) was measured. Even though, the disc has several holes only the time for one particular hole for one revolution is measured

over 30 revolutions. This corresponds to the measurement for a chopper disc with one hole. With that, the rotational speed stability together with the position control stability of the rotor can be measured separately with no influence of the manufacturing accuracy and the residual unbalance. The measurement showed a very low jitter of 6 ppm of the rotational speed. This jitter is inversely proportional with the rotational speed as shown in Figure 11.

The overall jitter due to manufacturing inaccuracies and operation of the chopper is below 4 ns for circumferential speeds above 650 m/s and rotational speeds above 200 krpm.
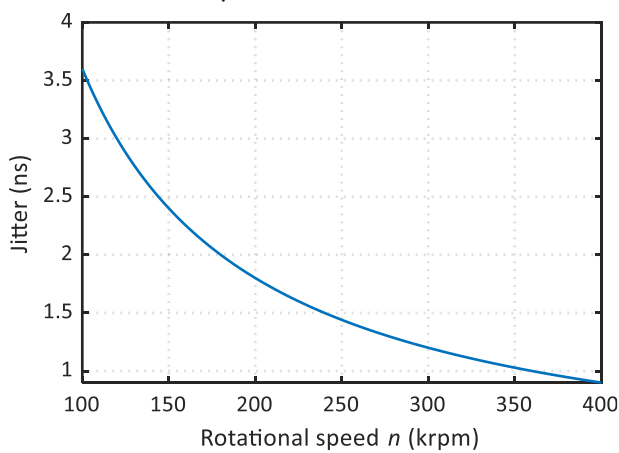

Figure 11: Jitter due to instability of the rotational speed and position control in function of the rotational speed.

4 Conclusion

For the design of ultra-high speed chopper rotors, different challenges have to be tackled. First, the chopper topology – parallel or perpendicular – is chosen. In a next step, the circumferential speed is calculated with the opening and closing time which is most often a given specification. The mechanical design reveals if the circumferential speed is feasible with regards to the material's strength. Within this white paper it is shown that a circumferential speed up to 1 km/s is possible for Stodola shaped rotor made from high-strength titanium. Furthermore, the rotor dynamics for the entire rotor have to be checked, namely the eigenfrequencies and the ratio of moments of inertia.

The jitter of the chopper system can rarely be influenced by the chopper rotor design. It is shown that the jitter is reduced with increasing rotational and circumferential speed. The jitter is mainly induced by the manufacturing accuracy, the balancing method and the accuracy of the speed and position control of the magnetic bearing system. For the magnetic bearing motor CM-AMB the jitter is below 4 ns for circumferential speeds above 650 m/s and rotational speeds above 200 krpm.

5 References

[1] M. D. Frogley, I. Lekkas, C. S. Kelley, and G. Cinque, "Performances for broadband synchrotron photothermal infrared nano-spectroscopy at Diamond Light Source," *Infrared Physics & Technology*, vol. 105, p. 103238, 2020, doi: 10.1016/j.infrared.2020.103238.

[2] M. Cammarata *et al.,* "Chopper system for time resolved experiments with synchrotron radiation," *The Review of scientific instruments*, vol. 80, no. 1, p. 15101, 2009, doi: 10.1063/1.3036983.

[3] M. Gembicky and P. Coppens, "On the design of ultrafast shutters for time-resolved synchrotron experiments," *Journal of synchrotron radiation*, vol. 14, Pt 1, pp. 133–137, 2007, doi: 10.1107/S0909049506041835.

[4] A. D. LeGrand, W. Schildkamp, and B. Blank, "An ultrafast mechanical shutter for X-rays," *Nuclear Instruments and Methods in Physics Research Section A: Accelerators, Spectrometers, Detectors and Associated Equipment*, vol. 275, no. 2, pp. 442–446, 1989, doi: 10.1016/0168-9002(89)90722-5.

[5] A. Stodola, *Dampf- und Gasturbinen: Mit Einem Anhang über die Aussichten der Wärmekraftmaschinen*. Berlin, Heidelberg, s.l.: Springer Berlin Heidelberg, 1924.